Noname manuscript No.
(will be inserted by the editor)

Effect of Weighting Full-field Residuals when Fitting Material Model Parameters

Charles F. Jekel · Martin P. Venter · Gerhard Venter · Raphael T. Haftka

Received: date / Accepted: date

Abstract A methodology is presented to fit material parameters in finite element (FE) models using full displacement field data. Four bulge inflation tests were performed on a PVC-coated polyester material. Digital image correlation (DIC) was used to capture the full displacement field of the material. An inverse analysis was set up to find material parameters in a FE model which replicated the full displacement field of the experimental test. Two different objective functions were considered to quantify the discrepancy between the FE model and test data. One function considered equal weight among displacement components, while the other function weighted the discrepancies to balance different displacement components. The resulting parameters, for isotropic and orthotropic models, were heavily dependent upon which objective function was chosen. Additionally, cross validation was performed to select between the two material models. Similar to the material parameters, the cross validation results preferred different material models depending upon which objective function was being used.

Keywords Inverse analysis · Objective functions · material parameter identification

1 Introduction

The finite element (FE) method has become an important design tool for membrane structures, and selecting material parameters to represent complex material behavior is a difficult task. This is especially true for the most complex and non-linear materials including coated woven fabrics. Inverse analyses, or iterative schemes for FE model updating (FEMU) have been used to find material parameters from complex load cases. In this paper, two different objective functions were investigated when

F. Author
first address
Tel.: +123-45-678910
Fax: +123-45-678910
E-mail: fauthor@example.com

S. Author
second address

estimating material parameters from bulge inflation tests on PVC-coated polyester. Objective function refers to how the discrepancy between the FE model and test data is quantified, and material parameters are typically selected to minimize this function. The objective function has an important effect on the material parameters selected using this type of inverse analysis (Zhan et al., 2011; Jekel et al., 2019; Tam, 2020).

PVC-coated polyester is a coated textile. It's most commonly modeled as a continuous, homogeneous, orthotropic material (Shaw et al., 2010), which is largely dependent on the warp-to-fill stiffness ratio (Dinh et al., 2017). The typical weave has the warp yarns pulled taut, while the fill yarns are woven in-between the warp yarns. The fill yarns run orthogonal to the warp yarns. Various non-linear models have been used in an attempt to better describe the behavior of the material. Galliot and Luchsinger (2009) proposed a non-linear material model based on the load ratio between the material warp and fill directions. Ambroziak and Kłosowski (2014) used a piecewise linear orthotropic model, and Jekel et al. (2017) used polynomials to describe the non-linear elastic behavior of the material.

Biaxial tests are commonly used to characterize material parameters for structural membrane materials (Stranghöner et al., 2016). Several studies (Rachik et al., 2001; Charalambides et al., 2002; Machado et al., 2012; Tonge et al., 2013) have used bulge (or bubble inflation) tests to induce an equal biaxial load on the material. These bulge tests typically involve inducing a pressure on one side of a circularly clamped membrane material. The equal biaxial load occurs at the apex of the deflected membrane for an isotropic material. The measured pressure and displacements are then used to infer material parameters, by comparing the results to a FE simulation.

A variety of applications (Becker et al., 2012; Murienne and Nguyen, 2016; Mejía and Lantsoght, 2016; Chisari et al., 2017) have used Digital image correlation (DIC) as non-invasive deformation measuring technique. The technique uses the correlation between consecutive images, from multiple cameras, to calculate a full 3D displacement field. For bulge tests, DIC is an ideal tool to obtain a full 3D displacement field while not interfering with the inflation or deflection of the membrane material.

Material parameters in various models have been identified using FEMU (Lovato et al., 1993; Cailletaud and Pilvin, 1994; Drass and Schneider, 2016). The process can be generalized by using optimization to find parameters in a FE model that minimize the discrepancy between the model and experimental data (Asaadi et al., 2017). In a forward problem parameters can be directly inferred from an experimental test. While an inverse problem iteratively updates the FE model to find parameters that lead to responses that resemble the experimental response (Lee et al., 2019). This process is often referred to as model calibration.

Model calibration can be performed using deterministic or probabilistic methods (Lee et al., 2019). A deterministic model calibration does not include the measurement uncertainty, while probabilistic method can account for both model and experimental uncertainty. Jung et al. (2016) stated that models calibrated deterministicly do not account for material uncertainty, and thus may result in unreliable solutions. The uncertainty of the experiments needs to be quantified in order to calibrate material models probalistically. Unfortunately, DIC displacement field data is typically treated as a black box where the uncertainties are not well understood. The bulge inflation tests is particularly challenging having out-of-plane displacements on the curved material surface. While it may be more reliable to calibrate the material model parameters using a probabilistic method, this work uses a deterministic

method because the uncertainty due to DIC errors of the displacement measurements is currently unknown. However, the experimental measurements are made available, so that a probabilistic calibration can be performed in the future.

There are many different choices of possible objective functions to calibrate material models. Zhan et al. (2011) proposed the EARTH method to calibrate model parameters into phase, magnitude, and slope errors from time history data. A single DIC bulge inflation test may generate over a hundred thousand unique time histories. In order to apply EARTH, each of these time histories would need to be broken into their respective errors and treated as separate objective functions in a multi-objective optimization. This process to compute the objective functions may be computationally expensive with lots of full-field data.

The previous studies (Rachik et al., 2001; Charalambides et al., 2002) used only the height to determine material parameters from bulge inflation tests. Machado et al. (2012) used curvatures to determine a stress tensor from bulge inflation tests to infer material parameters for an elastic material. While these previous methods work well for a planar isotropic material, they are difficult to extend to a directional dependent woven textile like PVC-coated polyester. Jekel et al. (2016) showed that it was possible to use the displacement field of a bulge test to select parameters for a non-linear orthotropic material model using simulated experimental data. Jekel (2016) then used this process on polynomial displacement fields fitted to experimental data at selected inflation pressures. These polynomial surfaces introduce an extra layer of error in the material parameters. This work will find material parameters by fitting the full experimental displacement field directly. A new approach is describe which allows for any data point in the experimental displacement field be compared to a FE model, for any initial surface location and inflation pressure. While (Jekel et al., 2016) considered the discrepancy in the x, y and z displacements fields to be equal weight, the objective function was dominated by the z displacements which were an order of magnitudes larger than the x and y components. Therefore, this work explores the effect of weighting down the z discrepancy.

This work also investigates using cross validation to select the best material model when performing FEMU. The idea is that cross validation could be used to determine whether the isotropic or orthotropic material model generalizes the PVC-coated polyester better in the complex load case. This is especially important for PVC-coated polyester, which is not a homogeneous (or continuous) material, but modeled as one in the FE method. Cross validation was performed using the two different objective functions described to select material parameters from the experimental data.

2 Methods

Bulge inflation tests were performed using DIC on PVC-coated polyester.[1] A FE model was created to replicate the boundary conditions of the bulge inflation tests. Two different objective functions are described. Each objective function represents a different method to quantify the difference between the experimental data and

[1] An online repository is available at `https://github.com/cjekel/inv_bubble_opt` which includes the source code to perform the inverse analysis, test data, and procedures to reproduce this work.

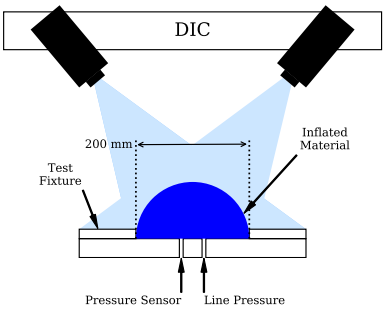

Fig. 1 Bulge inflation test overview.

FE model. The process to perform the inverse analysis is briefly described. Cross validation is also discussed as a method for selecting material models in this scheme.

2.1 Experimental tests

The bulge inflation tests involve clamping a sample of membrane material into a circular clamp. Pressure is then induced on one side of the material. The material deflections were recorded using DIC. The DIC system used was the StrainMaster with DaVis (LaVision GmbH, 2014), which was capable of syncing the inflation pressure with the recorded images. A visual representation of a bulge inflation test is provided in Figure 1.

Four bulge inflation tests were performed at Stellenbosch University in South Africa. Details of the process and test fixture are found in section 5.1 of (Jekel, 2016). The diameter of the circular bulge test was 200 mm. The PVC-coated polyester tested was Mehler Texnologies VALMEX® 7318 (the same material tested in(Jekel et al., 2017)). Four samples of material were cut from the same roll, with each sample being a 250 mm square. Spray paint was added to the surface of each specimen, with a random pattern, to increase the surface contrast of the material for DIC processing. Each test was inflated from zero to three bar, by manually opening a compressed air valve to the bulge inflation test fixture. This resulted in each test being inflated at a unique load rate as seen in Figure 2. The internal pressure was recorded with a Festo SPTE-P10R-S4-V-2.5K pressure transmitter.

Full field bulge inflation tests generated a large amount of data as shown in Table 1. The xy-plane was oriented with the surface of the material prior to inflation, with the x direction occurring in the warp material direction, while the y direction occurred in the fill material direction. The material was inflated in the z direction. The number of data points ranged from test to test. The variation was largely dependent on how finely the DIC data was processed. Here the largest test generated nearly two million data points, while the smallest test generated only two hundred thousand data points. Each data point represents a unique combination of inflation pressure p and initial x,y location. There are three deformations recorded for each data point, represented as separate $\Delta x, \Delta y$, and Δz values.

The DIC techniques were not perfect, as there are missing data points in some of the test. This happens when correlations is lost between images, and becomes more

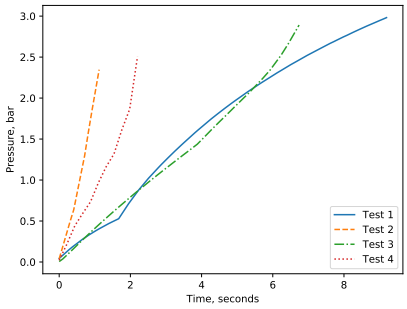

Fig. 2 Pressure time curves from each bulge inflation test.

Table 1 Number of unique (x, y, p) data points from each test and inflation pressures.

Test	# of data points
1	1,836,961
2	729,718
3	1,201,509
4	289,312

evident with larger deflections. Additionally, the severity of missing data varies from test to test. Figure 3 shows each x, y data point at the last inflation pressure of each test, where each colored pixel is a DIC data point. The spacing of the x, y data points vary from test to test as a result of different DIC processing While Tests 1 and 2 have the highest density of data points, Test 1 doesn't have any missing data points while test 2 has several small holes on the surface of the material. The worst of the missing data occurs with test 3, which has large holes on one quarter of the test. Test 4 only has two small holes on the surface of the data, and also has the least number of x, y data points on the surface of the material.

2.2 Finite Element model

An implicit non-linear FE model was constructed in ABAQUS which resembled the physical boundary conditions of the bulge inflation test. Sheplak and Dugundji (1998) described differential equations to solve for the displacement field of bulge inflation tests for isotropic and orthotropic material models, but (Sheplak and Dugundji, 1998) was not used as the geometry is simple enough to quickly construct in any non-linear FE code. The FE model uses an implicit solver, with 201 load steps between zero and three bar. Each load step uses adaptive time stepping. The adaptive time stepping allows the model to solve a single load-case in one step, or cut back to smaller increments if needed. Over 900 linear Q4 membrane elements are used to represent the surface of the material. The linear elements prevent nonphysical out-of-plane force imbalances. The displacement field at the nodes of the FE solver are exported to be used in further calculations when the model is run with a given material model.

The displacement field of the FE model needs to be computed several times at various pressures which correspond with the pressures of the experimental data. Either load steps can be added to the FE model at the exact experimental pressures, or the displacement field of the FE model can be interpolated to match the exact

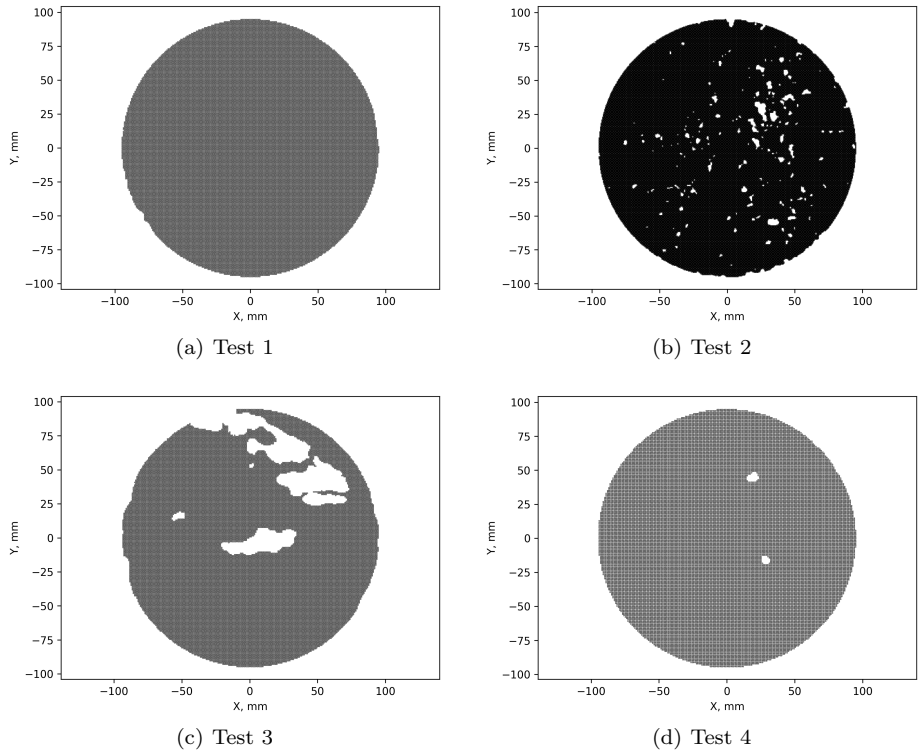

(a) Test 1 (b) Test 2

(c) Test 3 (d) Test 4

Fig. 3 Plots of the x,y data points of each bulge inflation test. The darker color is related to having a higher density of data points.

experimental pressures. Interpolation was chosen since it didn't involve manually editing the input deck for each test, and resulted in a fixed number of exported displacement fields. Specifically linear interpolation was used to evaluate the FE model's displacement at the nodes for the exact pressures of the experimental test. Linear interpolation is use to solve the displacement field $\Delta(x,y,p)$ by interpolating the displacement field at the two nearest pressures as

$$\frac{\Delta(x,y,p)-\Delta(x,y,p_1)}{p-p_1}=\frac{\Delta(x,y,p_2)-\Delta(x,y,p_1)}{p_2-p_1} \tag{1}$$

where p_2 and p_1 represent the nearest pressures of the FE models' load steps.

Overall, the linear interpolation scheme proved very accurate when interpolating between the FE model load steps. The linear interpolation accuracy was compared to FE models with load steps halfway in-between the previous 201 load steps (representing the worse possible interpolation case). The linear interpolation error was negligible, with the interpolation error following on the order of single precision (10^{-8} mm) numerical noise. This level of single precision was the same level of precision used by the FE model.

Linear isotropic and orthotropic material models were investigated. An isotropic model with one unknown parameter (stiffness modulus E), and an isotropic model with two unknown parameters (stiffness modulus E and the shear modulus G) were

considered. The orthotropic model was simplified as a three parameter mode, with parameters for the stiffness moduli (E_1 & E_2), and the shear modulus (G_{12}). The one parameter isotropic model and the orthotropic model use a Poisson's ratio of 0.24 as measured in (Jekel et al., 2017). Using a constant Poisson's ratio simplifies issues with gradient magnitudes, as it is anticipated that gradients of Poisson's ratio could be orders of magnitude different than stiffness moduli.

The displacement field of the FE model for an orthotropic material model at 2.0 bar is shown in Figures 4 through 6. The maximum Δz value is about ten times larger than the Δx or Δy values. Radial Basis Functions (RBF) are used to interpolate the displacements from the initial (x, y) node locations at each outputted pressure. The RBFs are exact at the node locations, and result in a smooth displacement field from the linear four node FE elements. The InterpolateSimpleRBF object construct these RBFs to the full displacement field of the FE analysis. The RBFs were inspired by the SciPy rbf function (Virtanen et al., 2020).

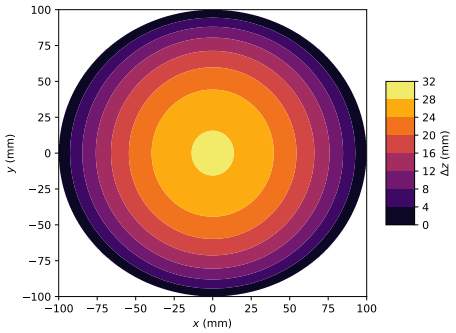

Fig. 4 Displacement Δz of FE model at 2.0 bar with orthotropic properties $E_1 = 0.8$ GPa, $E_2 = 0.15$ GPa, $G_{12} = 0.025$ GPa, and $\nu_{12} = 0.24$.

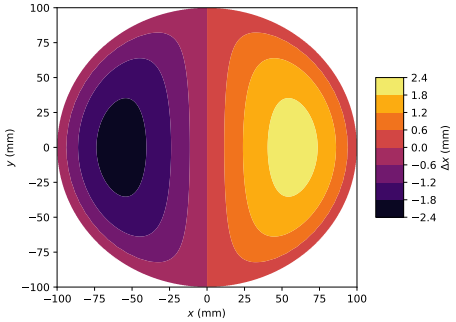

Fig. 5 Displacement Δx of FE model at 2.0 bar with orthotropic properties $E_1 = 0.8$ GPa, $E_2 = 0.15$ GPa, $G_{12} = 0.025$ GPa, and $\nu_{12} = 0.24$. Note the symmetry about $x = 0$.

The radial basis functions are expressed as

$$\boldsymbol{y} = \boldsymbol{A}\boldsymbol{\lambda} \tag{2}$$

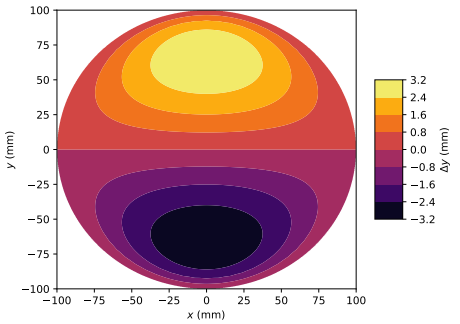

Fig. 6 Displacement Δy of FE model at 2.0 bar with orthotropic properties $E_1 = 0.8$ GPa, $E_2 = 0.15$ GPa, $G_{12} = 0.025$ GPa, and $\nu_{12} = 0.24$. Note the symmetry about $y = 0$.

where

$$\boldsymbol{A} = \begin{bmatrix} ||\boldsymbol{x}_1 - \boldsymbol{x}_1||_2 & ||\boldsymbol{x}_2 - \boldsymbol{x}_1||_2 & \cdots & ||\boldsymbol{x}_n - \boldsymbol{x}_1||_2 \\ ||\boldsymbol{x}_1 - \boldsymbol{x}_2||_2 & ||\boldsymbol{x}_2 - \boldsymbol{x}_2||_2 & \cdots & ||\boldsymbol{x}_n - \boldsymbol{x}_2||_2 \\ \vdots & \vdots & \ddots & \vdots \\ ||\boldsymbol{x}_1 - \boldsymbol{x}_n||_2 & ||\boldsymbol{x}_2 - \boldsymbol{x}_n||_2 & \cdots & ||\boldsymbol{x}_n - \boldsymbol{x}_n||_2 \end{bmatrix} \tag{3}$$

which follows a simple linear kernel (Broomhead and Lowe, 1988). The RBF parameters $\boldsymbol{\lambda}$ are solved for a general input of $\boldsymbol{x}$, output of $\boldsymbol{y}$, with n data points. Then $\hat{n}$ predictions are generated for new $\hat{\boldsymbol{x}}$ locations as

$$\hat{\boldsymbol{y}} = \hat{\boldsymbol{A}}\boldsymbol{\lambda} \tag{4}$$

where

$$\hat{\boldsymbol{A}} = \begin{bmatrix} ||\boldsymbol{x}_1 - \hat{\boldsymbol{x}}_1||_2 & ||\boldsymbol{x}_2 - \hat{\boldsymbol{x}}_1||_2 & \cdots & ||\boldsymbol{x}_n - \hat{\boldsymbol{x}}_1||_2 \\ ||\boldsymbol{x}_1 - \hat{\boldsymbol{x}}_2||_2 & ||\boldsymbol{x}_2 - \hat{\boldsymbol{x}}_2||_2 & \cdots & ||\boldsymbol{x}_n - \hat{\boldsymbol{x}}_2||_2 \\ \vdots & \vdots & \ddots & \vdots \\ ||\boldsymbol{x}_1 - \hat{\boldsymbol{x}}_{\hat{n}}||_2 & ||\boldsymbol{x}_2 - \hat{\boldsymbol{x}}_{\hat{n}}||_2 & \cdots & ||\boldsymbol{x}_n - \hat{\boldsymbol{x}}_{\hat{n}}||_2 \end{bmatrix}. \tag{5}$$

For this problem, $\boldsymbol{x}$ refers to the in-plane (x,y) location of the FE model nodes, $\hat{\boldsymbol{x}}$ refers to the in-plane (x,y) location of the DIC data, $\boldsymbol{y}$ denotes the displacement from the FE model, and $\hat{\boldsymbol{y}}$ represents the experimental displacements. This type of RBF is ideal for interpolating surfaces of FE models since it is exact at node locations, and results in a smooth interpolation in-between the FE node locations.

2.3 Objective functions

The objective function which quantifies the discrepancy between the physical bulge inflation tests and the FE model difference is fundamental for the optimization in the inverse analysis. The average absolute deviation between the x displacement of the FE model and inflation test is denoted $r_{\Delta x}(j,\boldsymbol{\beta})$ for the j test and $\boldsymbol{\beta}$ set of material

parameters. These average absolute deviations are expressed as

$$r_{\Delta x}(j,\boldsymbol{\beta}) = \frac{1}{n_j}\sum_{i=1}^{n_j} |\Delta x(x_i,y_i,p_i)_t - \Delta x(x_i,y_i,p_i,\boldsymbol{\beta})_f| \tag{6}$$

$$r_{\Delta y}(j,\boldsymbol{\beta}) = \frac{1}{n_j}\sum_{i=1}^{n_j} |\Delta y(x_i,y_i,p_i)_t - \Delta y(x_i,y_i,p_i,\boldsymbol{\beta})_f| \tag{7}$$

$$r_{\Delta z}(j,\boldsymbol{\beta}) = \frac{1}{n_j}\sum_{i=1}^{n_j} |\Delta z(x_i,y_i,p_i)_t - \Delta z(x_i,y_i,p_i,\boldsymbol{\beta})_f| \tag{8}$$

where n_j is the total number of data points in the j test. A simple discrepancy is then formulated as the average L_1 distance in mm as

$$e(\boldsymbol{\beta}) = \frac{1}{n_t}\sum_{j}^{n_t} r_{\Delta x}(j,\boldsymbol{\beta}) + r_{\Delta y}(j,\boldsymbol{\beta}) + r_{\Delta z}(j,\boldsymbol{\beta}) \tag{9}$$

where n_t is the total number of tests. The subscripts t is for the physical inflation test data, while the subscript f is from the FE model.

The formulation of e considers the discrepancy in the x, y, and z directions to have an equal weight. This formulation could be problematic if the discrepancy in one displacement components dominates the others. In the bulge inflation test data, the Δz component was roughly ten times larger than the in-plane (x or y) components. This creates the potential for the $r_{\Delta z}$ discrepancies to be larger than the other two directions, because the Δz values have the potential to be at least ten times larger than Δx or Δy.

A second objective function is proposed as e_w to deal with the imbalance between the maximum in-plane and out-of-plane displacements. The function is just a slight modification of e, and is expressed as

$$e_w(\boldsymbol{\beta}) = \frac{1}{n_t}\sum_{j}^{n_t} r_{\Delta x}(j,\boldsymbol{\beta}) + r_{\Delta y}(j,\boldsymbol{\beta}) + w r_{\Delta z}(j,\boldsymbol{\beta}) \tag{10}$$

where w is a weighting component[2]. While there can be many ways to select w, a simple scheme was chosen as

$$w_z = \frac{1}{n_t}\sum_{j}^{n_t} \frac{\max\left(\Delta x(j)\right) + \max\left(\Delta y(j)\right)}{2\max\left(\Delta z(j)\right)} \tag{11}$$

which represents the ratio of the average x and y displacement to the maximum z displacement. This resulted in $w = 0.1$ for the bulge inflation tests in consideration.

Two different objective functions are presented to quantify the difference between the full displacement field of the FE model and DIC tests. One objective function is an average L_1 norm between the x,y,z displacements, while the other function is a relative L_1 which considers the weighted difference between x,y and z displacements. A zero for both functions would indicate that the FE model's displacement field exactly matches the experimental data.

The optimization requires the objective function e or e_w to be computed multiple times. There are many steps required to automate this using software, and the process

[2] The software available online allows a weight to be specified for each directional component of the displacement field.

is described in Table 2. Several Python functions were created to interface with the the ABAQUS solver and post processor for this application. The function essentially returns e or e_w from inputted material parameters.

Table 2 Process to compute the objective function for given material parameters.

Step	Description
1	Write the material model parameters to the ABAQUS input file
2	Run ABAQUS solver on the input file
3	Run ABAQUS post processor to export displacement field of FE model
4	Load the FE displacement field into memory
5	Compute the discrepancy between FE model and DIC data: i) Linearly interpolate the FE model to match the pressures of the bulge test data ii) Construct and evaluate RBFs to the FE model displacement field iii) Compute $r_{\Delta x}$, $r_{\Delta y}$, and $r_{\Delta z}$ for each set of test data
6	Compute the final objective function of e or e_w

2.4 Optimization

The inverse analysis is the process of finding the material parameters of the FE model to match the bulge inflation test data. The optimization problem can be stated as

$$\text{minimize:} \quad e(\boldsymbol{\beta}) \tag{12}$$

$$\text{subject to:} \quad \beta_l \leq \beta_k \leq \beta_u, \quad k = 1, 2, \cdots, n_p. \tag{13}$$

where $\boldsymbol{\beta}$ is the vector of material parameters which are restricted to some reasonable lower and upper bounds. The isotropic parameters are expressed as $\boldsymbol{\beta} = (E)$ or $\boldsymbol{\beta} = (E, G)$, and the simplified orthotropic parameters are expressed as $\boldsymbol{\beta} = (E_1, E_2, G_{12})$. Note that e_w is substituted for e when minimizing the weighted objective function.

The first optimization strategy used a global optimizer with an allocated number of function evaluations. When the global optimizer exhausted the specified budget, a local optimizer was used for final convergence to a local optimum. The global optimization strategy used was Efficient Global Optimization (EGO), which utilized the expected improvement from a Gaussian process to minimize the function (Jones et al., 1998; The GPyOpt authors, 2016). A variant of the BFGS (Broyden, 1970; Fletcher, 1970; Goldfarb, 1970; Shanno, 1970) gradient based optimization was used as the local optimizer (Virtanen et al., 2020; Byrd et al., 1995). Initially 50 EGO function evaluations (calculations of e) were performed before switching to the BFGS implementation. A budget of 200 function evaluations for the BFGS appeared to be sufficient at finding a local optimum.

After several runs of the EGO to BFGS strategy, it became evident that the optimizer was failing at finding a global optimum. A multi-start optimization strategy was adopted to better deal with the presence of multiple local minima. The multi-start process ran five BFGS optimizations from different starting points in the design space (Schutte et al., 2006). Each of the five BFGS runs were limited to either 200 function evaluations, or satisfying the convergence criteria. Converge considered either relative changes in the objective function, absolute changes in the

objective function, or gradient magnitude. This multi-start optimization was able to consistently find better optimums than the EGO to BFGS strategy, but at the cost of additional objective functions.

There is the possibility that some combination of material parameters may cause the FE analysis to not converge. This is problematic when the optimization algorithm requires a discrepancy for a particular set of parameters that lead to failed convergence. To deal with this problem, the maximum objective value from the runtime history was passed to the optimization algorithm when the FE analysis failed to converge. Additionally, a discrepancy value of 30 mm was passed if the first function evaluation in a given run failed to converge. This strategy works well with EGO, however it creates a non-differential objective function which can be problematic for gradient based optimization algorithms. There are also problems with the use of a L_1 based objective function, where gradients can vanish when the residual of a single points goes to zero.

While there were a number of potential issues using gradient based optimization with this application, in practice the gradient optimization was able to successfully minimize the objective function. Looking at the optimization history, the FE analysis would only fail to converge during the line search stage of the gradient based optimization algorithm, and not the finite differences which approximate the gradients. This is less problematic because the gradients were accurate. Lastly, there were no observed issues with the optimization caused by the L_1 objective function.

2.5 Cross validation

Cross validation is a model selection or validation tool used in various regression problems to assess the quality of models (Queipo et al., 2005). Cross validation provides for a nearly unbiased estimate of the modeling error, and can be used to diagnose overfitting or bias errors. Cross validation can be used to compare the performance of one material model to another in the context of fitting material models with an inverse analysis (FEMU). This may be important in practice when the ideal material model is unknown. In this case, cross validation will be used to quantitatively compare how the linear isotropic and orthotropic material models represent the behavior of PVC-coated polyester from these bulge inflation tests.

The processes proposed is similar to leave-one-out cross validation, and is described in Table 3. This cross validation score was computed for both the linear isotropic and orthotropic material models. The model with the lower cross validation score is assumed to be a better generalized representation of the material behavior.

Table 3 Process to compute leave-one-test-out cross validation error.

Step	Description
1	Perform optimization without test j
2	Calculate the discrepancy e or e_w on the left-out test j
3	Repeat 1 & 2 for all tests
4	Cross validation score is the average discrepancy e or e_w from the left-out tests

3 Results

Inverse analyses were performed on the bulge inflation tests to find material parameters for the linear isotropic and linear orthotropic models. The results show parameters when each test were fit separately (such that $n_t = 1$). Lastly, the cross validation errors were computed by fitting parameters to all combinations of the three tests ($n_t = 3$). The focus of the results is to demonstrate the effect of the two objective functions.

3.1 Linear isotropic material model

Resulting parameters for the single parameter (E) linear isotropic material model are found in Table 4, and results for the two parameter model (E and G) are shown in Table 5. The one parameter model used a Poisson's ratio of 0.24, while optimization of the two parameter resulted in a Poisson's ratio near 0.5. Effectively the shear modulus in the two parameter model approached the lower limit[3], and the FE model is unable to run when the Poisson ratio exceed 0.5. Poisson's ratio appears to significantly effect the stiffness modulus E, in which the one parameter model resulted in a larger stiffness modulus. For both models there was little difference between parameters from minimizing e or e_w with the first test. The second and third test produced larger stiffness moduli when minimizing e_w, and the degree of the increase was larger with the one parameter model. In general, it appeared that minimizing e_w resulted in stiffer material parameters. Parameters of the two parameter isotropic model appears less effected by the weighted objective function than the single objective function.

Table 4 One parameter isotropic material results from each inverse analysis. Note ν was fixed to 0.24.

	Minimizing e	Minimizing e_w
	E (GPa)	E (GPa)
Test 1	0.279	0.283
Test 2	0.222	0.292
Test 3	0.242	0.282
Test 4	0.218	0.253

Table 5 Resulting isotropic material parameters from each inverse analysis. Note ν is calculated from E and G.

	Minimizing e			Minimizing e_w		
	E (GPa)	G (GPa)	ν	E (GPa)	G (GPa)	ν
Test 1	0.279	0.113	0.24	0.283	0.114	0.24
Test 2	0.160	0.054	0.48	0.170	0.057	0.48
Test 3	0.162	0.054	0.50	0.170	0.057	0.49
Test 4	0.154	0.052	0.48	0.155	0.052	0.49

The objective values from the various fits are shown in Table 6. For both objective functions, the fourth test resulted in the smallest objective values (or the best fit).

[3] The lower limit of G is $E/3$, and Poisson's ratio is expressed as $\nu = E/(2G) - 1$.

The largest objective values (or the worst fit test) depends upon which objective function was minimized, but appears to be either the second or third test. In most cases, the two parameter model resulted in lower objective function values than the one parameter model.

Table 6 Resulting objective values when fitting the linear isotropic models to each bulge inflation test.

	One parameter (E)		Two parameter (E, G)	
	e (mm)	e_w	e (mm)	e_w
Test 1	1.554	0.497	1.554	0.497
Test 2	1.881	0.795	1.699	0.725
Test 3	1.870	0.588	1.716	0.549
Test 4	1.195	0.457	1.054	0.403

3.2 Linear orthotropic material model

The simplified linear orthotropic material parameters resulting from inverse analysis on the individual tests are shown in Table 5. The parameters of the orthotropic model are very different depending upon which objective function was minimized. There are sizable changes to both E_1 and E_2 depending upon whether e or e_w was minimized. The most interesting changes occur in the second and third test, where the choice of objective function reversed the stiffness directions. Minimizing e resulted in $E_2 > E_1$, but minimizing e_w resulted in $E_1 > E_2$. Overall, minimizing e_w resulted in parameters that were more consistent from test to test which is expected since the test material was nominally identical. While the stiffness moduli were very different depending on e or e_w, the shear modulus was nearly the same in all conditions.

Table 7 Resulting orthotropic material parameters from minimizing tests independently with each inverse analysis. Note that ν_{12} was fixed to 0.24.

	Minimizing e (GPa)			Minimizing e_w (GPa)		
	E_1	E_2	G_{12}	E_1	E_2	G_{12}
Test 1	0.343	0.248	0.005	0.303	0.229	0.005
Test 2	0.212	0.241	0.004	0.306	0.230	0.005
Test 3	0.217	0.257	0.004	0.306	0.229	0.005
Test 4	0.239	0.215	0.004	0.280	0.215	0.005

The objective values resulting from each parameter set with the linear orthotropic model are shown in Table 8. The table shows the resulting values of e_w when e was minimized, and vice versa. The definition of the worse fit depends upon which objective function was minimized. In all cases, the value of e_w was worse when e was minimized than when e_w was minimized. A similar statement can be made for minimizing e_w. If we consider test two, the objective values when minimizing e changed up to 15% when minimizing e_w while E_1 changed over 40% when the objective function was changed.

Comparisons of the differences between the two parameter isotropic material model and the linear orthotropic material model are shown in Figures 7 through

Table 8 Objective values when minimizing e or e_w for the linear orthotropic model to each bulge inflation test.

	Minimizing e (GPa)		Minimizing e_w (GPa)	
	e (mm)	e_w	e (mm)	e_w
Test 1	1.550	0.512	1.773	0.490
Test 2	1.660	0.765	1.917	0.710
Test 3	1.702	0.570	1.759	0.527
Test 4	1.033	0.406	1.101	0.380

10. The chosen displacement locations occur at the approximate maximums for the linear orthotropic FE model, as previously shown in Figures 4 through 6. The Δ_x displacements occur at $[x = 56, y = 0]$, the Δ_y displacements occur at $[x = 0, y = 63]$, and the Δ_z displacements occur at $[x = 0, y = 0]$ on the surface of the material. The displacements were plotted with the inflation pressure. The results of the one parameter isotropic material model have been omitted, because they were nearly identical to the two parameter isotropic results with the same objective function.

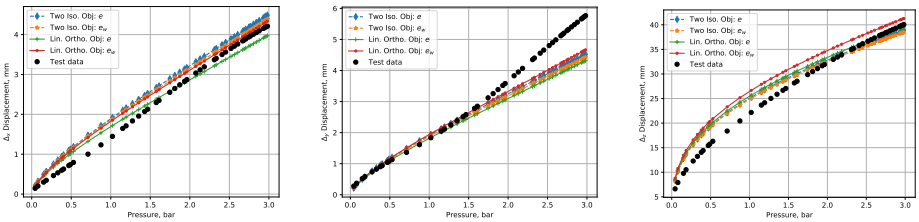

(a) Δ_x displacement (b) Δ_y displacement (c) Δ_z displacement

Fig. 7 Resulting displacements from the two parameter isotropic and the linear orthotropic material models compared with test 1. The Δ_x results shown in A) occur at $[x = 56, y = 0]$. The Δ_y results shown in B) occur at $[x = 0, y = 63]$. The Δ_z results shown in C) occur at $[x = 0, y = 0]$.

The linear orthotropic FE model appears to match the selected test data better than the isotropic model in all of the cases presented in Figures 7 through 10. Although it is unclear whether the choice of e or e_w as the objective function resulted in a better fits. It appears that the linear orthotropic model with e_w as the objective function matched the Δ_x and Δ_y displacements better, while the e objective function matched the Δ_z displacements better. There are exceptions to both of these cases, where the reverse is seen, depending on which test is considered.

The differences between e and e_w for the two parameter isotropic model were very subtle. However, there is a more noticeable difference between e and e_w for the linear orthotropic material model. This is most evident in the maximum Δ_z displacement pressure curves for all tests. The non-linearity of the Δ_z displacements is more prevalent than the Δ_x or Δ_y displacements.

3.3 Cross validation material model comparison

Inverse analyses were performed to fit isotropic and orthotropic material models to the bulge inflation tests. Additional inverse analyses were performed such that

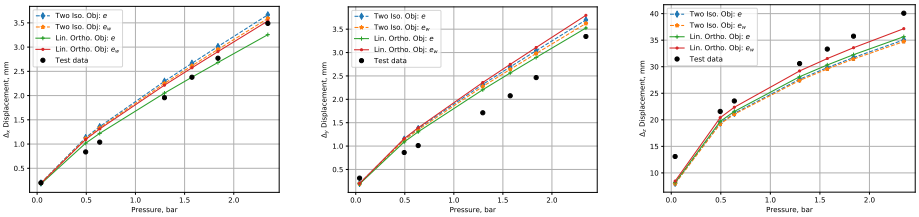

(a) Δ_x displacement (b) Δ_y displacement (c) Δ_z displacement

Fig. 8 Resulting displacements from the two parameter isotropic and the linear orthotropic material models compared with test 2. The Δ_x results shown in A) occur at $[x = 56, y = 0]$. The Δ_y results shown in B) occur at $[x = 0, y = 63]$. The Δ_z results shown in C) occur at $[x = 0, y = 0]$.

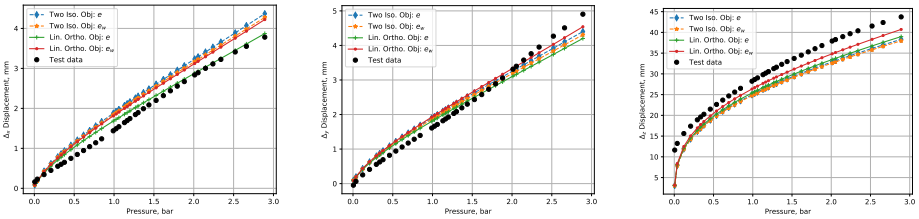

(a) Δ_x displacement (b) Δ_y displacement (c) Δ_z displacement

Fig. 9 Resulting displacements from the two parameter isotropic and the linear orthotropic material models compared with test 3. The Δ_x results shown in A) occur at $[x = 56, y = 0]$. The Δ_y results shown in B) occur at $[x = 0, y = 63]$. The Δ_z results shown in C) occur at $[x = 0, y = 0]$.

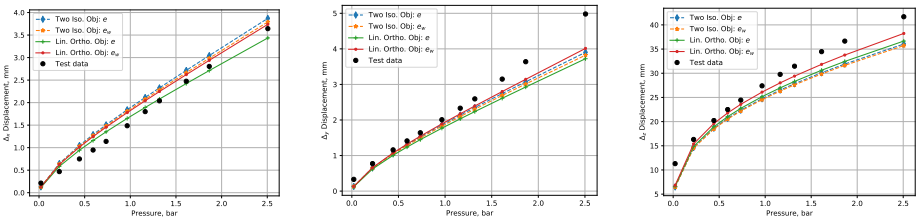

(a) Δ_x displacement (b) Δ_y displacement (c) Δ_z displacement

Fig. 10 Resulting displacements from the two parameter isotropic and the linear orthotropic material models compared with test 4. The Δ_x results shown in A) occur at $[x = 56, y = 0]$. The Δ_y results shown in B) occur at $[x = 0, y = 63]$. The Δ_z results shown in C) occur at $[x = 0, y = 0]$.

a leave-one-test-out cross validation score was computed for each material model. The resulting discrepancy values are presented in Table 9. The orthotropic material model had the lowest cross validation error when e_w was minimized, but the two parameter isotropic material model had the lowest cross validation error when e was minimized. The different objective functions appear to prefer different material models. This implies that the material model which generalizes the bulge inflation test better depends on the definition of the discrepancy between the test data and FE model.

The two parameter isotropic material model parameters from the full inverse analysis and the cross validation runs are presented in Table 10. When e was min-

Table 9 Resulting discrepancy from the inverse analysis and leave-one-test-out cross validation.

	Cross validation error		Left out test values	
Model	e (mm)	e_w	e [1, 2, 3, 4]	e_w [1, 2, 3, 4]
isotropic (E)	1.995	0.590	[2.47, 2.10, 1.87, 1.54]	[0.62, 0.52, 0.59, 0.63]
isotropic (E and G)	1.833	0.554	[2.37, 1.85, 1.72, 1.40]	[0.57, 0.50, 0.56, 0.60]
orthotropic	1.856	0.533	[2.47, 1.88, 1.73, 1.35]	[0.49, 0.72, 0.53, 0.40]

imized, the stiffness modulus varied from 0.155 to 0.170 GPa. However, when e_w was minimized the stiffness modulus varied from 0.170 to 0.193 GPa. and the shear modulus varied from 0.057 to 0.070 GPa. Overall, e_w resulted in more consistent and stiffer moduli.

Table 10 Resulting two parameter isotropic material parameters from each inverse analysis.

	Minimizing e (GPa)		Minimizing e_w (GPa)	
	E	G	E	G
Leaving test 1 out	0.155	0.052	0.170	0.057
Leaving test 2 out	0.167	0.056	0.170	0.057
Leaving test 3 out	0.164	0.055	0.170	0.056
Leaving test 4 out	0.170	0.057	0.193	0.066

The orthotropic material parameters from the cross validation study are shown in Table 11. There is a significant difference between the parameter variance depending upon which objective function was used. For instance, E_1 varied from 0.224 to 0.280 GPa when e was minimized. However, when e_w was minimized E_1 varied from 0.303 to 0.305 GPa. A similar trend occurs for E_2 and G_{12}, where minimizing e_w resulted in more consistent parameters.

Table 11 Resulting orthotropic material parameters from each inverse analysis.

	Minimizing e (GPa)			Minimizing e_w (GPa)		
	E_1	E_2	G_{12}	E_1	E_2	G_{12}
Leaving test 1 out	0.224	0.235	0.003	0.303	0.229	0.005
Leaving test 2 out	0.297	0.231	0.004	0.304	0.229	0.005
Leaving test 3 out	0.284	0.224	0.004	0.304	0.229	0.005
Leaving test 4 out	0.280	0.244	0.003	0.305	0.229	0.005

4 Discussion

The most striking result was the effect of the two objective functions on selecting parameters for the linear orthotropic material model. When e was minimized the linear orthotropic parameters varied significantly from test to test, with some tests resulting in $E_2 > E_1$ and others $E_1 > E_2$. This was not the case when e_w was minimized, in which the parameters from test to test were fairly consistent with $E_1 > E_2$. The difference between the two objective functions was that e considered the discrepancies in the x,y and z directions to be of equal weight, while e_w considered the

z discrepancies to be one tenth the weight. This weighting factor corresponds to an imbalance between the test maximum z displacement being about ten times larger than the maximum x or y displacements. It's important to clarify that both e and e_w would approach zero if it was possible for a perfect fit, however resulting material parameters occur with the inability to perfectly fit the data. In these circumstances it appears that one may need to careful consider how to eventuate the discrepancy of the displacement field, especially under similar imbalanced displacement data.

Tests two and three are of particular interest with the linear orthotropic model, because these tests resulted in $E_2 > E_1$ when e was minimized. It could be reasonable to assume that the test directions were incorrect by a factor of 90°, and that this mistake in the x and y directions resulted in the set of parameters. Additional inverse analyses were performed on these tests, where the test data was rotated by factors of 45° and 90°. What is interesting is that when e was minimized the resulting parameters resulted in $E_2 > E_1$ regardless of the rotation, and there was little change to the parameters. However, when e_w was minimized both E_2 and E_1 would change significantly based on the rotation. This hints that giving more weight to the x and y displacements, like in e_w, would be better if an inverse analyses was required to identify orthotropic parameters without knowing the primary and secondary material directions.

The different objective functions had an interesting effect on using leave-one-test-out cross validation for material model selection. When e was minimized, the cross validation error favored the two parameter isotropic material model. Though when e_w was minimized, the cross validation error favored the orthotropic material model by a much larger margin. This reemphasizes the importance of selecting an appropriate objective function, as the choice of objective function not only effects the resulting parameters, but also effects the perceived generalization error of the model.

5 Conclusion

An inverse analysis was described to find material parameters by matching the full displacement field from bulge inflation tests. Optimization was used to find material parameters in a FE model that best matched the experimental displacement field from tests on PVC-coated polyester. Material parameters were determined for a linear isotropic and simplified linear orthotropic material models. Two different objective functions were considered to describe the discrepancy between the experimental data and numerical model. The first objective function considered equal weight between the displacement components, while the other function gave more weight to the x and y displacements. The weighting scheme was chosen to compensate for the fact that the majority of the deflections within the bulge inflation test occur out-of-plane. Resulting material parameters for the linear orthotropic material model were very different depending on which objective function was minimized. Thus the choice of objective function being considered is very important when performing such an optimization on the full field data.

Cross validation was performed to determine whether the isotropic or orthotropic material model was a better representation of the material behavior. There was little difference in the cross validation error according to the equally weighted objective function, however the weighted objective function heavily favored the orthotropic

material model. This indicates that the choice of objective function was not only important in material parameter selection, but can also impact material model selection.

Acknowledgements Thanks to Sudharshan Udhayakumar for help constructing the FE model and comparing the FE model to analytical solutions. Thanks to Andrés Bernardo for helping set up script to process the full displacement field data.

Replication of results

The FE models require a commercial code to run. Experimental data, Python scripts to perform the optimization, and FE model input decks are available online with instructions at `https://github.com/cjekel/inv_bubble_opt`

Declarations

Funding

Charles F. Jekel has received the following funding for his PhD research which has supported this work: University of Florida Graduate Preeminence Award, U.S. Department of Veterans Affairs Educational Assistance, and Stellenbosch University Merrit Bursary.

Conflicts of interest

The authors declare that they have no conflict of interest.

Availability of data and material

The experimental data is available online with instructions on how to download at `https://github.com/cjekel/inv_bubble_opt`

Code availability

The scientific Python ecosystem was used to produce these results. Specific scripts used to perform the optimizations are available online at `https://github.com/cjekel/inv_bubble_opt`

References

Ambroziak A, Kłosowski P (2014) Mechanical properties for preliminary design of structures made from PVC coated fabric. Construction and Building Materials 50:74–81, DOI 10.1016/j.conbuildmat.2013.08.060

Asaadi E, Wilke DN, Heyns PS, Kok S (2017) The use of direct inverse maps to solve material identification problems: pitfalls and solutions. Structural and Multidisciplinary Optimization 55(2):613–632, DOI 10.1007/s00158-016-1515-1, URL https://doi.org/10.1007/s00158-016-1515-1

Becker TH, Mostafavi M, Tait RB, Marrow TJ (2012) An approach to calculate the J-integral by digital image correlation displacement field measurement. Fatigue & Fracture of Engineering Materials & Structures 35(10):971–984, DOI 10.1111/j.1460-2695.2012.01685.x, URL https://onlinelibrary.wiley.com/doi/abs/10.1111/j.1460-2695.2012.01685.x

Broomhead DS, Lowe D (1988) Radial basis functions, multi-variable functional interpolation and adaptive networks. Tech. rep., Royal Signals and Radar Establishment Malvern (United Kingdom)

Broyden CG (1970) The Convergence of a Class of Double-rank Minimization Algorithms 1. General Considerations. IMA Journal of Applied Mathematics 6(1):76–90, DOI 10.1093/imamat/6.1.76, URL https://dx.doi.org/10.1093/imamat/6.1.76

Byrd RH, Lu P, Nocedal J, Zhu C (1995) A limited memory algorithm for bound constrained optimization. SIAM Journal on Scientific Computing 16(5):1190–1208

Cailletaud G, Pilvin P (1994) Identification and inverse problems related to material behaviour. Inverse problems in engineering mechanics 1:79–86

Charalambides M, Wanigasooriya L, Williams G, Chakrabarti S (2002) Biaxial deformation of dough using the bubble inflation technique. I. Experimental. Rheologica Acta 41(6):532–540, DOI 10.1007/s00397-002-0242-2

Chisari C, Macorini L, Amadio C, Izzuddin BA (2017) Optimal sensor placement for structural parameter identification. Structural and Multidisciplinary Optimization 55(2):647–662, DOI 10.1007/s00158-016-1531-1, URL https://doi.org/10.1007/s00158-016-1531-1

Dinh TD, Rezaei A, Daelemans L, Mollaert M, Hemelrijck DV, Paepegem WV (2017) A hybrid micro-meso-scale unit cell model for homogenization of the nonlinear orthotropic material behavior of coated fabrics used in tensioned membrane structures. Composite Structures 162:271–279, DOI https://doi.org/10.1016/j.compstruct.2016.12.027, URL http://www.sciencedirect.com/science/article/pii/S0263822316313204

Drass M, Schneider J (2016) On the mechanical behavior of transparent structural silicone adhesive–TSSA. In: SEMC 2016–Sixth International Conference on Structural Engineering, Mechanics and Computation, pp 14–16

Fletcher R (1970) A new approach to variable metric algorithms. The Computer Journal 13(3):317–322, DOI 10.1093/comjnl/13.3.317, URL https://dx.doi.org/10.1093/comjnl/13.3.317

Galliot C, Luchsinger R (2009) A simple model describing the non-linear biaxial tensile behaviour of PVC-coated polyester fabrics for use in finite element analysis. Composite Structures 90(4):438–447, DOI 10.1016/j.compstruct.2009.04.016

Goldfarb D (1970) A family of variable-metric methods derived by variational means. Math Comp 24 (1970), 23-26 DOI https://doi.org/10.1090/S0025-5718-1970-0258249-6

Jekel CF (2016) Obtaining non-linear orthotropic material models for PVC-coated polyester via inverse bubble inflation. Master's thesis, Stellenbosch University, URL http://hdl.handle.net/10019.1/98627

Jekel CF, Venter G, Venter MP (2016) Obtaining a hyperelastic non-linear orthotropic material model via inverse bubble inflation analysis. Structural and Multidisciplinary Optimization pp 1–9, DOI 10.1007/s00158-016-1456-8, URL http://dx.doi.org/10.1007/s00158-016-1456-8

Jekel CF, Venter G, Venter MP (2017) Modeling PVC-coated polyester as a hypoelastic non-linear orthotropic material. Composite Structures 161:51–64, DOI http://dx.doi.org/10.1016/j.compstruct.2016.11.019, URL http://www.sciencedirect.com/science/article/pii/S0263822316320839

Jekel CF, Venter G, Venter MP, Stander N, Haftka RT (2019) Similarity measures for identifying material parameters from hysteresis loops using inverse analysis. International Journal of Material Forming 12(3):355–378, DOI 10.1007/s12289-018-1421-8, URL https://doi.org/10.1007/s12289-018-1421-8

Jones DR, Schonlau M, Welch WJ (1998) Efficient Global Optimization of Expensive Black-Box Functions. Journal of Global Optimization 13(4):455–492, DOI 10.1023/A:1008306431147, URL https://doi.org/10.1023/A:1008306431147

Jung BC, Yoon H, Oh H, Lee G, Yoo M, Youn BD, Huh YC (2016) Hierarchical model calibration for designing piezoelectric energy harvester in the presence of variability in material properties and geometry. Structural and Multidisciplinary Optimization 53(1):161–173, DOI 10.1007/s00158-015-1310-4, URL https://doi.org/10.1007/s00158-015-1310-4

LaVision GmbH (2014) Product-Manual DaVis 8.2 Software, 8th edn. Göttingen, Germany

Lee G, Kim W, Oh H, Youn BD, Kim NH (2019) Review of statistical model calibration and validation—from the perspective of uncertainty structures. Structural and Multidisciplinary Optimization 60(4):1619–1644, DOI 10.1007/s00158-019-02270-2, URL https://doi.org/10.1007/s00158-019-02270-2

Lovato G, Moret F, Le Gallo P, Cailletaud G, Pilvin P (1993) Determination of brazed joint constitutive law by inverse method. Le Journal de Physique IV 3(C7):C7—-1135

Machado G, Favier D, Chagnon G (2012) Membrane curvatures and stress-strain full fields of axisymmetric bulge tests from 3D-DIC measurements. Theory and validation on virtual and experimental results. Experimental mechanics 52(7):865–880

Mejía CA, Lantsoght EOL (2016) Strain and deflection analysis in plain concrete beams and reinforced concrete beams by applying Digital Image Correlation. In: SEMC 2016–Sixth International Conference on Structural Engineering, Mechanics and Computation, CRC Press

Murienne BJ, Nguyen TD (2016) A comparison of 2D and 3D digital image correlation for a membrane under inflation. Optics and Lasers in Engineering 77:92–99, DOI https://doi.org/10.1016/j.optlaseng.2015.07.013, URL http://www.sciencedirect.com/science/article/pii/S0143816615001888

Queipo NV, Haftka RT, Shyy W, Goel T, Vaidyanathan R, Kevin Tucker P (2005) Surrogate-based analysis and optimization. Progress in Aerospace Sciences 41(1):1–28, DOI 10.1016/j.paerosci.2005.02.001, URL http://www.sciencedirect.com/science/article/pii/S0376042105000102

Rachik M, Schmidtt F, Reuge N, Le Maoult Y, Abbeé F (2001) Elastomer biaxial characterization using bubble inflation technique. II: Numerical investigation of some constitutive models. Polymer Engineering & Science 41(3):532–541, DOI 10.1002/pen.10750, URL https://onlinelibrary.wiley.com/doi/

abs/10.1002/pen.10750

Schutte JF, Haftka RT, Fregly BJ (2006) Improved global convergence probability using multiple independent optimizations. International Journal for Numerical Methods in Engineering 71(6):678–702, DOI 10.1002/nme.1960, URL https://doi.org/10.1002/nme.1960

Shanno DF (1970) Conditioning of quasi-Newton methods for function minimization. Math Comp 24 (1970), 647-656 DOI https://doi.org/10.1090/S0025-5718-1970-0274029-X

Shaw A, Sriramula S, Gosling PD, Chryssanthopoulos MK (2010) A critical reliability evaluation of fibre reinforced composite materials based on probabilistic micro and macro-mechanical analysis. Composites Part B: Engineering 41(6):446–453, DOI https://doi.org/10.1016/j.compositesb.2010.05.005, URL http://www.sciencedirect.com/science/article/pii/S1359836810000818

Sheplak M, Dugundji J (1998) Large Deflections of Clamped Circular Plates Under Initial Tension and Transitions to Membrane Behavior. Journal of Applied Mechanics 65(1):107–115, URL http://dx.doi.org/10.1115/1.2789012

Stranghöner N, Uhlemann J, Bilginoglu F, Bletzinger KU, Bögner-Balz H, Corne E, Gibson N, Gosling P, Houtman R, Llorens J, Others (2016) Prospect for European Guidance for the Structural Design of Tensile Membrane Structures. Science and Policy Report (SaP-Report) Draft Version To be published by the Joint Research Centre (JRC) of the European Commission, publication expected

Tam JH (2020) Identification of elastic properties utilizing non-destructive vibrational evaluation methods with emphasis on definition of objective functions: a review. Structural and Multidisciplinary Optimization DOI 10.1007/s00158-019-02433-1, URL https://doi.org/10.1007/s00158-019-02433-1

The GPyOpt authors (2016) GPyOpt: A bayesian optimization framework in python. http://github.com/SheffieldML/GPyOpt

Tonge TK, Atlan LS, Voo LM, Nguyen TD (2013) Full-field bulge test for planar anisotropic tissues: Part I – Experimental methods applied to human skin tissue. Acta Biomaterialia 9(4):5913–5925, DOI https://doi.org/10.1016/j.actbio.2012.11.035, URL http://www.sciencedirect.com/science/article/pii/S1742706112005983

Virtanen P, Gommers R, Oliphant TE, Haberland M, Reddy T, Cournapeau D, Burovski E, Peterson P, Weckesser W, Bright J, van der Walt SJ, Brett M, Wilson J, Jarrod Millman K, Mayorov N, Nelson ARJ, Jones E, Kern R, Larson E, Carey C, Polat I, Feng Y, Moore EW, Vand erPlas J, Laxalde D, Perktold J, Cimrman R, Henriksen I, Quintero EA, Harris CR, Archibald AM, Ribeiro AH, Pedregosa F, van Mulbregt P, Contributors S (2020) SciPy 1.0: Fundamental Algorithms for Scientific Computing in Python. Nature Methods DOI https://doi.org/10.1038/s41592-019-0686-2

Zhan Z, Fu Y, Yang RJ, Peng Y (2011) An automatic model calibration method for occupant restraint systems. Structural and Multidisciplinary Optimization 44(6):815–822, DOI 10.1007/s00158-011-0671-6, URL https://doi.org/10.1007/s00158-011-0671-6